Meteorol Atmos Phys 92, 83–93 (2006)
DOI 10.1007/s00703-005-0139-6

Meteorology and Atmospheric Physics
Printed in Austria

Department of Atmospheric Sciences, Institute of Astronomy, Geophysics and Atmospheric Sciences, University of São Paulo, São Paulo, Brazil

Determination of O_3-, CO- and PM_{10}-transport in the metropolitan area of São Paulo, Brazil through synoptic-scale analysis of back trajectories

O. R. Sánchez-Ccoyllo, P. L. Silva Dias, M. de Fátima Andrade, and **S. R. Freitas**

With 6 Figures

Received December 6, 2004; revised December 28, 2004; accepted March 11, 2005
Published online: September 20, 2005

Summary

This study is aimed to qualitatively analyze the impact of remote sources on air pollution in the Metropolitan Area of São Paulo (MASP). Air-mass back trajectories from June to August of 1999 were calculated using a three-dimensional kinematic trajectory model and grouped into trajectory clusters. Correlations of individual trajectory clusters with O_3, CO and PM_{10} concentrations were determined. In this model, trajectories were obtained using the means of the three wind velocity components (U, V and W). The three-dimensional wind field was derived from the Regional Atmospheric Modeling System, and downscaling was employed. Coarse and fine nested grids (64-km and 16-km horizontal resolution, respectively) were used. Every 12 h (at 00 and 12 UTC), a back-trajectory ensemble, using the 64-km grid, was calculated for five defined endpoints at intervals of 0.5° N, S, E and W of the MASP ($\lambda = 23°33'$S, $\varphi = 46°45'$W), that last endpoint being centered in the MASP. To analyze cluster trajectories, the five trajectory ensembles from each day were allocated into one of four clusters (northeast, southeast, southwest or northwest quadrant) based on the origin of the trajectory over 4 days. Days on which all five trajectories originated from the same quadrant were classified as ''core'' days. Core day concentrations of CO, O_3 and PM_{10} during the study period were evaluated. The results show that, during the study period, air-mass back trajectories in the MASP originated from all four quadrants: northeast (32%), southeast (12%), southwest (19%) and northwest (37%). Our analysis of back-trajectory clusters in the MASP suggests a transport to ambient air of O_3 precursors and O_3 from the northeast region, which is associated with agricultural activities involving biomass burning.

1. Introduction

The Metropolitan Area of São Paulo (MASP) is the largest industrialized city in South America and is currently home to approximately 18 million inhabitants (CETESB, 2004). Therefore, in the MASP, human activities have an enormous impact on air quality, as well as on public health (Saldiva et al, 1995). Due to the progressive expansion of the MASP, aerosols have become a subject ever-greater interest to those involved in assessing atmospheric air quality. In the MASP, there are numerous heavy industries (such as iron and steel works), cement factories, refineries and chemical manufacturing facilities, as well as sulfuric acid and petrochemical plants. In addition, the automotive fleet now exceeds 7.5 million vehicles (CETESB, 2004) and is the main source of air pollutant emissions. The MASP presents an unconventional mixture of vehicle types, in which a variety of fuel blends, including oxygenated ones (gasoline with 22% alcohol) and pure ethanol (used in the light-duty fleet) are burned (CETESB, 2000). According to

Montero et al (2001), direct vehicle emissions seem to be the primary source of formaldehyde and acetaldehyde in the MASP in the morning, whereas at midday and in the evening these compounds appeared to be formed mainly by photochemical processes. The authors showed that secondary photochemical production of organic acids and aldehydes is more pronounced in the MASP atmosphere from midday to evening, particularly on days with strong solar radiation. Furthermore, vehicular emissions are the most significant sources of polycyclic aromatic hydrocarbons in the urban area of the MASP (Vasconcellos et al, 2003). A study using LIDAR data showed the presence of aerosols at altitudes of approximately 1500–2000 m, corresponding to the upper part of the planetary boundary layer over the MASP (Landulfo et al, 2003). Although local sources have a huge impact, it is believed that remote sources contribute to aerosol emissions of pollutants from fossil fuel combustion, as well as from biomass burning.

On the other hand, the back trajectories from a receptor site are commonly used to identify air pollution source regions and specific sources (Salvador et al, 2004; Tsuang, 2003; Lupu and Maenhaut, 2002; Man and Shih, 2001; Stohl, 1996). The analysis of back trajectories provides more detailed information on local conditions immediately prior to sampling, as well as on the history of the previous several days (Cape et al, 2000).

The goal of this study was to examine the influence of the remote sources on inhalable particulate matter (PM_{10}), carbon monoxide (CO) and ozone (O_3) concentrations in the MASP. This study applies methodologies proposed by Brankov et al (1998), Cape et al (2000) and Man and Shih (2001) and combines several techniques, namely, back-trajectory analysis, cluster analysis and correlation analysis. The techniques were applied in order to determine remote source contributions to air pollutant concentrations in the area. The study analyzed three months (June, July and August of 1999) of data regarding PM_{10}, CO and O_3 concentrations measured at several locations in the MASP. The first step in the methodology was to calculate the back trajectories using a three-dimensional kinematic trajectory model (Freitas et al, 1996; 2000). Cluster analysis was then applied to the trajectories according to their origin by quadrant (four quadrants related to wind direction). Pollutant concentrations were then separated by trajectory cluster. Finally, correlations were determined between individual clusters and transport of PM_{10}, CO and O_3 in the MASP. Herein, we present the methodology and discuss the results of its application to the PM10, CO and O_3 data from several monitoring locations in the MASP (Fig. 1).

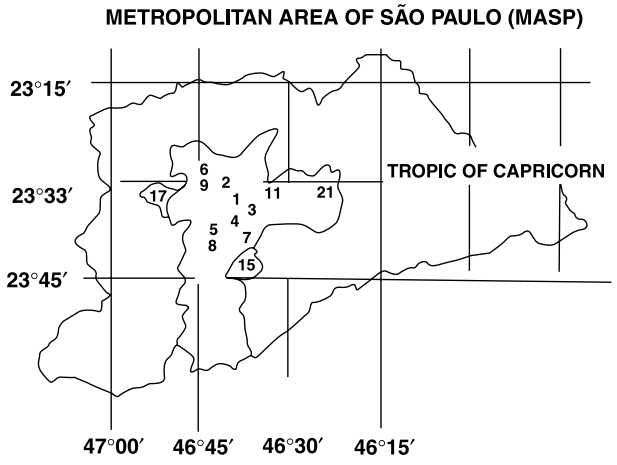

Fig. 1. Map of the Metropolitan Area of São Paulo (MASP) and monitoring stations: 1 Parque Dom Pedro II (PDP), 2 Santana, 3 Moóca, 4 Cambuci, 5 Ibirapuera, 6 Nossa Senhora de Ó, 7 São Caetano do Sul (SCS), 8 Congonhas, 9 Lapa, 11 Penha, 15 Diadema, and 21 São Miguel Paulista (SMP)

2. Methods

2.1 Computation of trajectories

Calculation of air trajectories is one the most frequently used methodologies for investigating regional-scale pollution problems. Ideally, trajectories trace the path of a polluted air parcel over a period of time. When the trajectory model is run backward in time, it can be used to identify the potential source regions of the pollutants measured at a receptor (Brankov et al, 1998).

In this study, the four day (96-h) back trajectories were computed by integration of the trajectory equations (Seibert, 1993; Stohl, 1998; Salvador et al, 2004):

$$\frac{dr}{dt} = v(r(t)) \tag{1}$$

assuming an initial value $r(t_0) = r_0$, $r(t)$ denotes the position vector at time t, and v the wind velocity vector (zonal wind, U, meridional wind, V and vertical wind, W). One numerical solution of the dif-

ferential equations, see Eq. (1), for computation of trajectories using a three-dimensional kinematic method has been developed (Freitas et al, 1996; 2000). The trajectory computation uses the iterative scheme (Pettersen, 1940). It can be described mathematically by the following recursive formulas (Stohl, 1998; Innocentini, 1999; Seibert, 1993), assuming a three-dimensional flow:

$$r_1^{(1)} = r_0 + v_{00}\Delta t, \qquad \Delta t \equiv (t_1 - t_0)$$

$$r_1^{(2)} = r_0 + 0.5\Delta t \times \left(v_{00} + v_{11}^{(1)}\right), \qquad v_{11}^{(1)} \equiv v\left(r_1^{(1)}, t_1\right)$$

$$\cdots$$

$$r_1^{(n)} = r_0 + 0.5\Delta t \times \left(v_{00} + v_{11}^{(n-1)}\right), \qquad v_{11}^{(n-1)} \equiv v\left(r_1^{(n-1)}, t_1\right).$$

The superscripts indicate the number of iterations. Let t_0 and t_1 be two time steps and the velocity be given by two functions of space $v(r, t_0)$ and $v(r, t_1)$, respectively. First, an arrival position r_1 of the parcel at $t = t_1$ is computed assuming a constant velocity of $v_0 = v(r_0, t_0)$. Since the velocity (U, V and W) at r_1 is $v_{11} \equiv v(r_1, t_1)$, a new arrival position is computed with a constant mean velocity $0.5(v_{00} + v_{11})$. This recursive method ends when convergence is achieved and the numerical solution is accurate to the second order (Seibert, 1993). The trajectory model has been coded using Fortran and the time integration can be performed in forward or backward modes alike.

For these simulations, the air parcel trajectory integration consists of 6-min time steps and provides the time evolution of the latitude, longitude and altitude above sea level.

Back trajectories arriving at an altitude of 1.5 km were chosen to define the impact of the local topography (Man and Shih, 2001; Salvador et al, 2004). In order to allow for uncertainty in the trajectory analysis, five trajectories were generated with arrival times at 00 UTC and 12 UTC, for endpoints at intervals of 0.5° N, S, E and W of the MASP (23°33′S, 46°39′W), the last endpoint centered in the MASP. The basic data set therefore comprised 905 three-dimensional trajectories.

In this study, the three-dimensional kinematic trajectory model (TM) and the Regional Atmospheric Modeling System (RAMS; Cotton et al, 2003) were linked in order to calculate the air parcel trajectories. Within this framework, RAMS produces a numerical simulation of the mean wind velocity (U, V and W), and the TM then calculates the trajectory of a parcel of air. The following section describes the RAMS meteorological model.

2.2 The atmospheric numerical model

Three-dimensional and non-hydrostatic, RAMS is a model for numerical simulation of atmospheric processes (Cotton et al, 2003). It employs multiple grid nesting and resolves the equations of motion, heat, moisture, and mass continuity using a terrain-following coordinate system. It supports parameterization of turbulence, shortwave and longwave radiation, sub-grid cumulus convection and microphysics data. For the boundary conditions, it uses 4DDA, allowing the atmospheric fields to be nudged toward the large-scale data.

For the RAMS model simulation discussed herein, the model domain and grid configurations are shown in Fig. 2, in which a 64-km horizontal grid covers almost the entire continent of South America, and a 16-km nested grid covers the MASP. This grid nesting was chosen in order to obtains high spatial resolution in selected areas, while covering a larger domain at lower resolu-

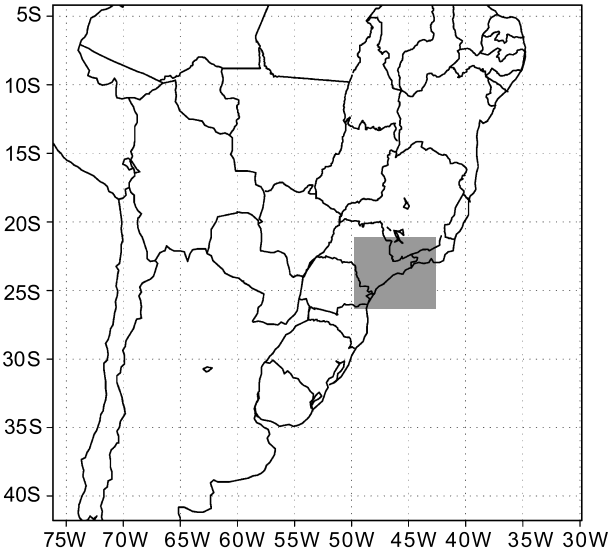

Fig. 2. RAMS simulation domain and grid configuration. The coarse grid and fine nested grid (shaded) intervals are 64 km and 16 km, respectively

tion (Pielke et al, 1992; Clark and Farley, 1984; Clark and Hall, 1991; Walko et al, 1995a). The model has 32 vertical levels, 60 meters thick at the surface and stretching to 1000 meters thick at 22.1 km, the domain top. The simulations span the period from 1 June 1999 through 31 August 1999. The model used 72-second time steps for the 64-km grid and 24-second time steps for the 16-km grid. The pole point for the oblique polar-stereographic projection was defined as 23°33′S latitude and 53° W longitude.

The model was initialized and updated in the lateral boundaries every 6 h by using the Center for Weather Forecasting and Climate Studies (CPTEC) analysis at 1.875° latitude by 1.875° longitude and 14 vertical standard pressure levels, from 1000 hPa to 30 hPa (Cavalcanti et al, 2002). The assimilated variables were zonal and meridional wind velocity, absolute temperature, relative humidity, geopotential and atmospheric pressure at sea level, which are interpolated from the CPTEC analysis grid onto the specified spatial grid resolution (Camargo and Silva Dias, 2000; Silva Dias and Machado, 1997).

The four-dimensional data assimilation of coarse-resolution analyzed fields in the RAMS was performed through Newtonian relaxation (Stauffer and Seaman, 1994) within five nudging points at the lateral boundary. Moreover, the lateral boundary nudging was conducted based on the Klemp-Wilhelmson condition, which applies only to the normal velocity component (U at the east and west boundaries). In this condition, the normal velocity component specified at the lateral boundary is effectively advected from the interior assuming a propagation speed. In contrast, the present study employed the relaxation time scales: 1800-second lateral boundary; 10800-second top of domain; and 86400-second center of domain. Parameterization of the horizontal diffusion coefficients was performed using the K-theory according to the formula devised by Smagorinsky (1963). The vertical diffusion was parameterized according to the Mellor and Yamada (1982) theory, which employs a prognostic equation for turbulent kinetic energy. The soil model used included equations for the diffusion of heat and moisture (Trembak and Kesller, 1985). The bulk cloud microphysics parameterization (i.e., level 3) was activated for cloud water and rain. In addition, the precipitation processes (Walko et al, 1995b), in which the water vapor in excess of saturation is assumed to condense, was included. The amount of precipitation was then computed and removed from the saturated layer by applying precipitation efficiency estimation (Meyer et al, 1997). The Kuo (1974) convection parameterization (Tremback, 1990) was also used. For the shortwave and longwave radiation parameterization, we used the technique developed by Harrington (1997), in which each form of hydrometeor (cloud water, rain, pristine ice, snow, aggregate, graupel and hail) and water vapor are accounted for.

The simulation used 6 soil layers, the bases of which were at 0.05 m, 0.175 m, 0.70 m, 1.50 m and 2.0 m. The surface-layer fluxes of heat, momentum and water vapor were computed using the method described by Louis (1979). The sea-surface temperature (SST) data used to initialize each grid was obtained from the Comprehensive Ocean-Atmosphere Data Set-COADS (Woodruff

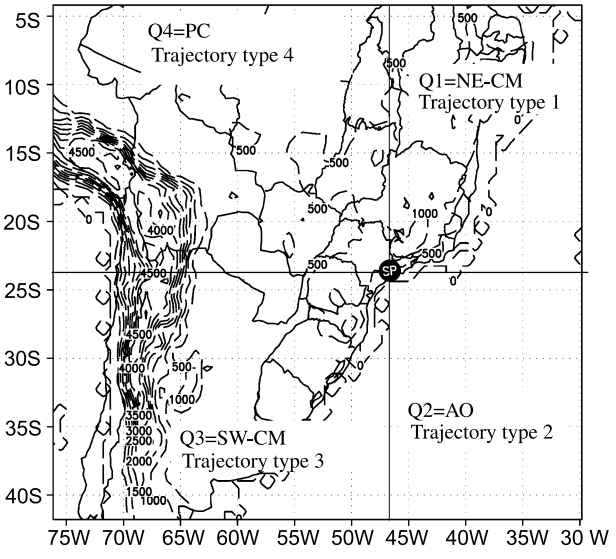

Fig. 3. The topographic distribution for the coarse grid in Fig. 2 and the area of origin of the back trajectories within each cluster: the northeast cluster (NE-CM), southeast cluster (AO), southwest cluster (SW-CM) and northwest cluster (PC); where NE-CM is the origin of back trajectories from northerly to east-northeasterly flows (N, NNE, NE and ENE), AO is the origin of back trajectories from easterly to west-southwesterly flows (E, ESE, SE, and SSE), SW-CM is the origin of back trajectories from southerly to west-southwesterly flows (S, SSW, SW, and WSW), and PC is the origin of back trajectories from westerly to north-northwesterly flows (W, WNW, NW, and NNW)

et al, 1998). The COADS contains the global monthly climatological SST data at a 1-degree (approximately 100-km) resolution and climatological values for each month of the year (Woodruff et al, 1998). Therefore, the climatological values from June to August of 1999 were used. The topographic distribution for the coarse grid in Fig. 2 is given in Fig. 3 (note that the coarse grid, at 64-km horizontal resolution, was chosen to calculate the synoptic air-mass back trajectories). In the RAMS, the sub-model topography is defined using a global, 30 arc-second (approximately 1-km resolution) topography dataset (Gesch et al, 1999), also available from the United States Geological Survey (USGS; Liston and Pielke, 2001). The vegetation data used was taken from standard products in the RAMS model package, which contains the global land-use data for RAMS version 4.3 at 30-second (approximately 1-km) resolution. The model vegetation distribution was defined using the International Geosphere-Biosphere Programme land-cover classification, available through the USGS Earth Resources Observation Satellite Data Center (http://edcdaac.usgs.gov/glcc/glcc.html). The USGS data set is based on 1-km Advanced Very High Resolution Radiometer data (http://www.atmet.com). Initial soil moisture distributions were generated through including spatially-constant soil moisture content over the domain.

2.3 Cluster analysis of air parcel back trajectories in the MASP

Cluster analysis is a multivariate statistical technique that splits a data set into a number of (preferably homogeneous) groups that should be as distinctly different from each other as possible (Brankov et al, 1998). In the present study, we developed the technique of combining cluster analysis and trajectory analysis, based on defining the geographic origin of the trajectory as one of four quadrants (Andrade et al, 1994; Poissant et al, 1996; Herrmann and Hanel, 1997). The origin of each air-mass back trajectory was identified as the northeast, southeast, southwest or northwest quadrant. These clusters, designated Q1 (trajectory type 1), Q2 (trajectory type 2), Q3 (trajectory type 3) and Q4 (trajectory type 4), respectively, are shown in Fig. 3, and wind direction (origin of the trajectory) is indicated.

Regions of origin of the air-mass back trajectories were grouped into Q1, Q2, Q3 and Q4 clusters, and correlations of the clusters with air pollutant concentrations were determined for the same period of the in trajectory calculation. These trajectories were calculated daily at 00 UTC and 12 UTC. At these hours, five trajectories were computed, and each five-trajectory hourly ensemble was examined. When all five trajectories originated from within the same quadrant, then that hourly data were retained as belonging to a ''core'' day (Cape et al, 2000). Core day results were later evaluated in order to understand the influence of atmospheric transport, according to trajectory cluster, on CO, O_3 and PM_{10} concentrations measured from June through August of 1999 at several monitoring stations over the MASP. It is of note that the clustering method proposed herein is based on geographical data only and does not depend upon information regarding levels or sources of pollutant concentrations.

2.4 Measurement of aerosol concentrations in the MASP

Mass concentrations of inhalable particulate matter with aerodynamic diameter less than 10 μm (PM_{10}) were measured continuously by the São Paulo State Environmental Protection Agency (CETESB; Alonso et al, 1997). The data were obtained using a Beta Gauge particulate monitor. Five monitoring stations within the MASP were chosen to sample PM_{10} concentrations from June to August of 1999. These air pollution monitoring stations are distributed throughout the MASP: Cambuci (23°33′47″, 46°36′28″, 740 m asl), Santana (23°32′50″, 46°38′10″, 730 m asl), Diadema (23°40′24″, 46°36′46″, 800 m asl), Nossa Senhora do Ó (Nsenhora; 23°28′28″, 46°40′18″, 720 m asl) and Penha (23°30′41″, 46°30′53″, 700 m asl).

2.5 Measurement of CO and O_3 concentrations in the MASP

The O_3 data set analyzed in this study consisted of daily 1-h maximum concentrations, obtained from the CETESB air quality monitoring network over a three-month period from June to August of 1999 (Alonso et al, 1997; CETESB,

2000). Six monitoring stations within the MASP were chosen for sampling of O_3 data: São Miguel Paulista (SMP; 23°30′00″, 46°27′30″, 800 m asl), São Caetano do Sul (SCS; 23°38′47″, 46°35′27″, 740 m asl), Parque Dom Pedro II (PDP; 23°32′43″, 46°37′45″, 730 m asl), Osasco (23°31′40″, 46°46′27″, 720 m asl), Ibirapuera (Ibira; 23°34′55″, 46°39′25″, 750 m asl), and Moóca (23°32′50″, 46°36′00″, 740 m asl).

The CO data set analyzed in this study consisted of hourly mean concentrations obtained from CETESB air quality monitoring stations. For CO data sampling, seven stations were chosen: PDP, SCS, Lapa (23°30′40″, 46°41′40″, 720 m asl), Congonhas (Congo; 23°36′29″, 46°39′37″, 760 m asl), Cerqueira César (César; 23°32′42″, 46°40′18″, 780 m asl), Centro (23°32′45″, 46°38′35″, 740 m asl) and Ibira.

3. Results

3.1 Classification of back trajectories in the MASP

Back trajectories of air masses arriving in the MASP at 00 UTC and 12 UTC were categorized into four types of trajectories depending on the origin of the air mass, as previously described. The location of origin (latitude, longitude and altitude) of the air-mass back trajectories were determined for the preceding four days (96 h). Trajectories originating in the northeast region of continental Brazil or in the Atlantic Ocean northeast of Brazil were categorized as Northeast Continental Marine (NE-CM; trajectory type 1 = Q1). Trajectory type 2 consisted of trajectories originating over the Atlantic Ocean (AO = Q2) and entering the MASP from the (southeast) coast. The last type was Southwest Continental Marine (SW-CM; trajectory type 3 = Q3) and represented trajectories originating in the southwestern quadrant of South America (Argentina, Uruguay, the Brazilian states of Parana and Porto Alegre, etc.) and over the Atlantic Ocean south of Brazil, moving into the MASP from the southwest. The designation Purely Continental (PC; trajectory type 4 = Q4) was used to describe trajectories originating within the South American Continent and moving directly into the MASP from the northwest (Fig. 3). Examples of the trajectory clusters are shown in Fig. 4.

Three-dimensional back trajectories calculated for the June–August 1999 period were analyzed

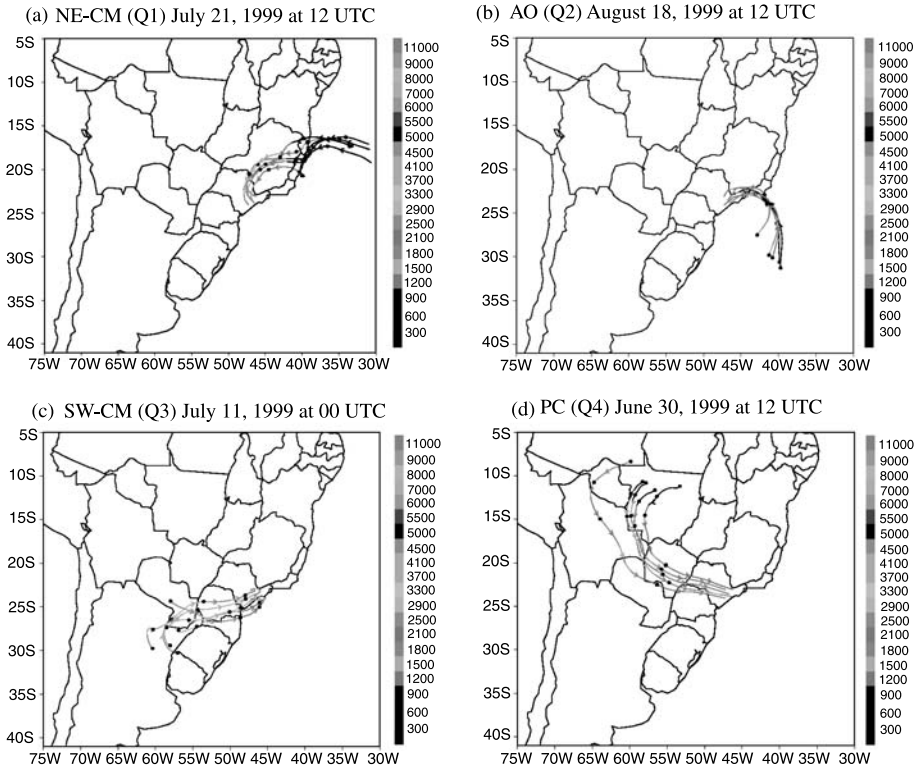

Fig. 4. Examples of the trajectory clusters described in Fig. 3: (**a**) NE quadrants, designated NE-CM; (**b**) SE quadrants, designated AO; (**c**) SW quadrants, designated SW-CM; and (**d**) NW quadrants, designated PC

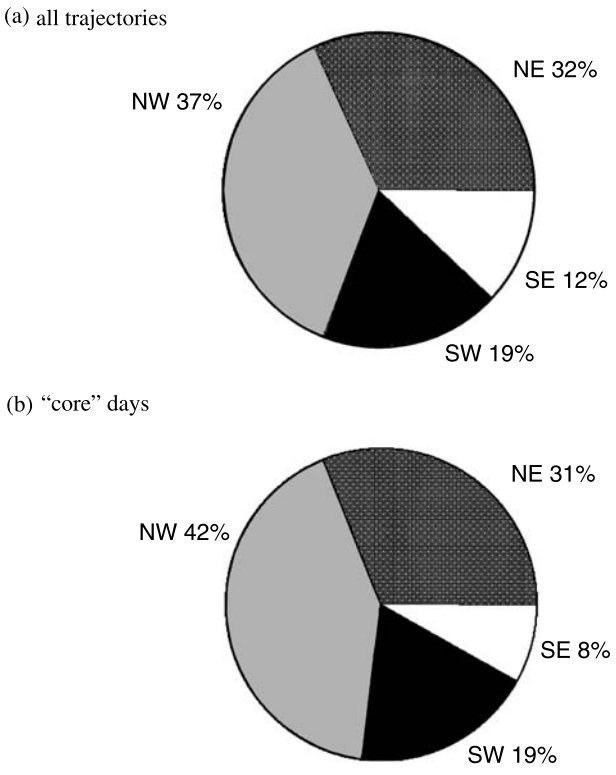

Fig. 5. Frequency of the different types of air-mass trajectories: (**a**) all trajectory cluster origins; (**b**) trajectory cluster origins for days on which all five trajectory ensembles at 0.5° latitude and longitude from the MASP were assigned to a single cluster, considering both 00 UTC and 12 UTC readings (''core'' days)

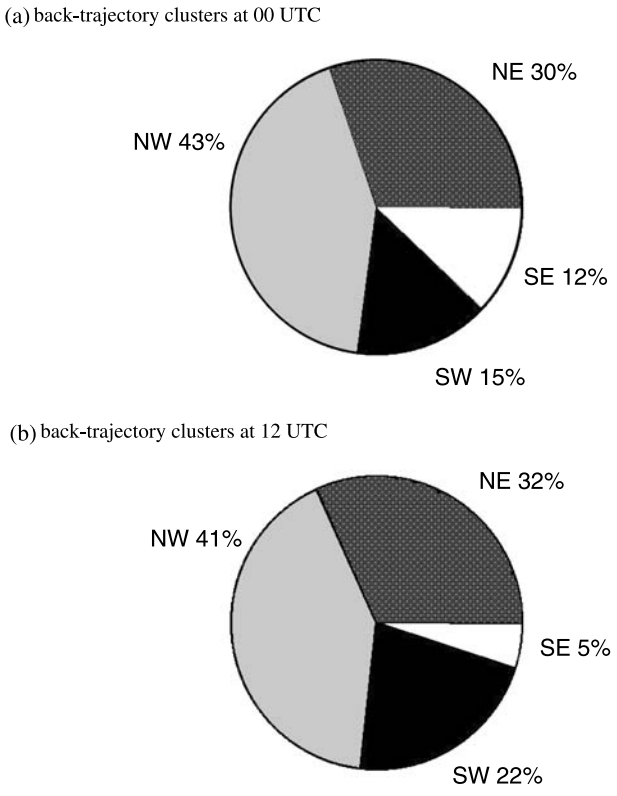

Fig. 6. Frequency of the different types of air-mass trajectories: (**a**) all trajectory cluster origins; (**b**) trajectory cluster origins for days on which all five trajectory ensembles at 0.5° latitude and longitude from the MASP were assigned to a single cluster, considering 00 UTC and 12 UTC readings separately (independent ''core'' days)

in order to identify the origins of the air parcels. Of the 905 trajectories calculated, 32% were type NE-CM (Q1), 12% were type AO (Q2), 19% were type SW-CM (Q3), and 37% were type PC (Q4) (Fig. 5a).

From all days in the data set, 74 were identified as core days (trajectory cluster). In 31% of these core days, the trajectories for both 00 UTC and 12 UTC were from the northeast quadrant (NE-CM = Q1), compared with 8% from the southeast (Q2 = AO), 19% from the southwest quadrant (SW-CM = Q3), 42% from the northwest quadrant (PC = Q4) (Fig. 5b).

The same trajectory analysis was performed for 00 UTC or 12 UTC independently, resulting in independent core days for 00 UTC and 12 UTC separately. At 00 UTC, we identified 33 core days. Of those 33 core days, 30% presenting trajectories originating in the northeast quadrant (NE-CM = Q1), 12% presented trajectories originating in the southeast quadrant (AO = Q2), compared with 15% presenting trajectories originating in the southwest quadrant (SW-CM = Q3), 43% presenting trajectories originating in the northwest quadrant (PC = Q4) (Fig. 6a). For 12 UTC, 41 days were designated core days. Of those, 32% presented trajectories from the northeast quadrant (NE-CM = Q1), 5% presented trajectories from the southeast quadrant (AO = Q2), 22% presented trajectories from the southwest quadrant (SW-CM = Q3), 41% presented trajectories from the northwest quadrant (PC = Q4), (Fig. 6b).

These results were correlated to the measured concentrations of O_3, CO and PM_{10}s using 5-h averages (2 h before, on the hour and 2 h after the 00 UTC and 12 UTC readings).

3.2 PM_{10} concentrations measured for different types of trajectories

The average PM_{10} concentrations at different stations and for different trajectory types are shown

Table 1. Means and standard deviations of PM_{10} concentrations (in $\mu g\, m^{-3}$) measured at different CETESB monitoring stations for the different types of air mass trajectories calculated at 00 UTC

	Cambuci	Santana	Diadema	Nsenhora	Penha
NE	65 (31)	70 (28)	50 (38)	74 (40)	68 (29)
SE	42 (25)	73 (14)	34 (10)	56 (34)	51 (18)
SW	38 (16)	58 (16)	19 (12)	51 (37)	37 (19)
NW	44 (19)	59 (19)	31 (17)	45 (27)	48 (30)

Nsenhora: Nossa Senhora do Ó

Table 2. Means and standard deviations of PM_{10} concentrations (in $\mu g\, m^{-3}$) measured at different CETESB monitoring stations for the different types of air mass trajectories calculated at 12 UTC

	Cambuci	Santana	Diadema	Nsenhora	Penha
NE	55 (33)	70 (20)	42 (28)	50 (29)	52 (26)
SE	53 (14)	73 (0.5)	36 (10)	63 (6)	40 (15)
SW	51 (23)	69 (13)	44 (24)	52 (17)	49 (25)
NW	46 (37)	53 (15)	41 (38)	48 (31)	40 (24)

Nsenhora: Nossa Senhora do Ó

in Tables 1 and 2. Table 1 presents the trajectory analysis of core days at 00 UTC. Figure 1 shows the locations of the various monitoring stations. As can be seen, the Cambuci station is situated in the central part of the MASP. Table 1 shows that PM_{10} concentrations measured at the Cambuci station were highest in air masses arriving from the northeast, as found for the other stations. It is expected also for other PM_{10}-measuring stations (Diadema, Nsenhora and Penha) greater mixtures of remote and local sources of PM_{10}s under the northeast flow influence. The main local sources of aerosol emissions in the urban area of the MASP were identified as resuspended soil dust, industrial emissions, motor vehicles, oil combustion, garbage incineration, vegetation, and sulfates. This was achieved through the use of receptor models (Sánchez-Ccoyllo and Andrade, 2002; Castanho and Artaxo, 2001; Andrade et al, 1994).

The clusters corresponding to the trajectories calculated at 12 UTC are shown in Table 2. No apparent indication of long-range transport aerosol from a specific direction (remote region) to the MASP is seen. This finding may be attributed to the potentially stable boundary layer and low velocity wind during the night.

3.3 O_3 and CO concentrations measured for different types of trajectories

The comparison of different trajectory clusters with O_3 concentrations at 00 UTC presented in Table 3 led to the identification of four different ozone concentration levels at the SMP station. Northeastern trajectory transport scenarios were found to result in significantly higher O_3 concentrations at the SMP station, whereas southeast, southwest, and northwest trajectory flows resulted in lower O_3 concentrations. As

Table 3. Means and standard deviations of O_3 concentrations (in $\mu g\, m^{-3}$) measured at different CETESB monitoring stations for the different types of air mass trajectories calculated at 00 UTC

	SMP	SCS	PDP	Osasco	Ibira	Moóca
NE	39.7 (22.7)	28.9 (18.1)	13.2 (5.6)	7.8 (4.6)	48.1 (31.9)	18.1 (15.1)
SE	18.4 (14.4)	19.3 (14.2)	5.3 (5)	7.9 (2.9)	50.9 (34.7)	25.2 (14.9)
SW	30.2 (12)	19.6 (10.9)	15.1 (4.8)	9.5 (3.7)	57.8 (37.7)	15.6 (10.5)
NW	18.5 (8.6)	14.3 (10.9)	13.2 (8.3)	9.1 (3)	28.0 (25.4)	11.9 (10.6)

SMP: São Miguel Paulista; SCS: São Caetano do Sul; PDP: Parque Dom Pedro II; Ibira: Ibirapuera

Table 4. Means and standard deviations of O_3 concentrations (in $\mu g\, m^{-3}$) measured at different CETESB monitoring stations for the different types of air mass trajectories calculated at 12 UTC

	SMP	SCS	PDP	Osasco	Ibira	Moóca
NE	34.1 (15.1)	34.3 (16.6)	17.7 (7.1)	12.3 (3.4)	22.4 (21)	26.0 (16.4)
SE	11.4 (1)	18.9 (0.6)	8.8 (3.5)	13.6 (2)	14.0 (3)	10.4 (3.1)
SW	19.8 (11.7)	19.3 (8)	13.9 (5.9)	11.4 (2.9)	12.7 (5.5)	13.8 (8.1)
NW	16.8 (7.6)	17.3 (7.5)	13.3 (7.2)	10.8 (2.9)	42.0 (30.3)	12.9 (7.6)

SMP: São Miguel Paulista; SCS: São Caetano do Sul; PDP: Parque Dom Pedro II; Ibira: Ibirapuera

Table 5. Means and standard deviations of CO concentrations (in ppm) measured at different CETESB monitoring stations for the different types of air mass trajectories calculated at 00 UTC

	PDP	SCS	Lapa	Congonhas	César	Centro	Ibira
NE	3.1 (2)	2.8 (1.9)	4.0 (2.9)	4.8 (2.2)	2.7 (1.7)	4.0 (2.6)	2.2 (1.6)
SE	2.1 (0.9)	2.5 (0.9)	2.0 (0.8)	3.8 (0.9)	2.5 (0.6)	2.9 (1.1)	1.6 (0.6)
SW	1.5 (1)	1.4 (0.9)	1.7 (1.6)	3.2 (1.3)	2.0 (1.6)	2.5 (1.5)	1.2 (1)
NW	2.3 (0.8)	2.1 (1.2)	2.4 (1.6)	3.5 (1.1)	2.4 (1.1)	2.7 (1)	1.5 (0.8)

PDP: Parque Dom Pedro II; SCS: São Caetano do Sul; César: Cerqueira César; Ibira: Ibirapuera

Table 6. Means and standard deviations of CO concentrations (in ppm) measured at different CETESB monitoring stations for the different types of air mass trajectories calculated at 12 UTC

	PDP	SCS	Lapa	Congonhas	César	Centro	Ibira
NE	1.8 (1.1)	1.8 (1.1)	2.5 (1.8)	3.2 (2)	2.3 (1.2)	2.1 (0.8)	1.2 (0.8)
SE	1.6 (0.6)	1.7 (0.7)	2.2 (1.1)	2.0 (0.9)	3.0 (1.1)	2.0 (0.5)	1.2 (0.5)
SW	2.2 (1.3)	1.8 (1)	2.8 (1.4)	4.0 (2.1)	3.1 (1.6)	2.7 (1.2)	1.8 (1.3)
NW	1.9 (1.3)	1.9 (1.5)	2.4 (1.5)	3.4 (1.8)	2.6 (1.4)	2.6 (1.2)	1.4 (1.1)

PDP: Parque Dom Pedro II; SCS: São Caetano do Sul; César: Cerqueira César; Ibira: Ibirapuera

seen in Fig. 1, the SMP station is situated in the northeast part of the MASP. At the other O_3-monitoring stations (SCS, PDP, Osasco, Ibira and Moóca), the highest impact on O_3 concentration was the local emission of its precursors. The same behavior was observed at the SMP site at 12 UTC (Table 4). At the other stations, the concentrations were mainly attributable to local sources such as vehicular traffic, industrial emissions and other urban sources. Under NW flow, it is plausible to assume that O_3 concentrations should be lower at SCS as well as in all other stations situated downstream of the MASP areas with intense emission of the O_3 precursors. Under SW or SE trajectories, O_3 concentration is expected to be lower because there are no significant areas with significant emission of precursors (except in the SE case that could eventually bring precursors from Cubatào. However, under these circumstances, cloudiness is expected to increase and therefore solar radiation is significantly reduced.)

In the different types of trajectories (NE-CM, AO, SW-CM and PC trajectory clusters), we observed no long-range transport of CO from remote areas into MASP at 00 UTC or 12 UTC. Therefore, the concentrations of pollutants in the MASP are predominantly determined by local sources, i.e., vehicular emissions (Tables 5 and 6).

4. Conclusions

The cluster analysis of the air mass back trajectories arriving in the MASP at 00 UTC and 12 UTC, from June to August of 1999 showed 4 different types of trajectory origin: 32% were from the northeast quadrant, designated the NE trajectory cluster; 12% were from the southeast quadrant, designated the SE trajectory cluster; 19% were from the southwest quadrant, desig-

nated the SW trajectory cluster; and 37% were from the northwest quadrant, designated the NW trajectory cluster.

From the back trajectory clusters calculated at 00 UTC, we identified 33 core days, of which 30% presented trajectories originating in quadrant NE, 12% presented trajectories originating in quadrant SE, 15% presented trajectories originating in quadrant SW, 43% presented trajectories originating in quadrant NW. From those calculated at 12 UTC, we identified 41 core days: 32% with trajectories from quadrant NE, 5% with trajectories from quadrant SE, 22% with trajectories from quadrant SW, 41% with trajectories from quadrant NW.

The air quality of the MASP depends on the contribution from many different sources, being the most important the vehicular emission, responsible for the emission of 40% of particles smaller than 10 μm. Other important sources are secondary reactions, i.e., gas-to-particle conversion, condensation and coagulation, contributing to 25% of PM_{10}. Soil dust resuspension generates 25% of these particles and the other 10% are due to industrial process emission (Miranda et al, 2002). For gaseous compounds, the participation of mobile sources to its concentration is more significant, approximately 90% of the ozone precursors are emitted to the atmosphere by the vehicular fleet.

For Particulate Matter, higher concentrations were found for Q1 trajectories at 00UTC, indicating that it can occur some transport from the Northeast part of the state to the center of the city. The main contribution to particulate concentration seems to come from local sources.

It is important to remember that the measurements of the pollutants concentrations used here were obtained at the surface level. There is a lack of information concerning vertical profiles of gaseous compounds and particulate matter concentrations. The vertical profiles could evaluate the transport from higher levels to surface.

Acknowledgments

This study has been conducted as part of project 'Meteorology and air pollution in São Paulo' supported by the Fundação de Amparo à Pesquisa de São Paulo (FAPESP; Project 96\0143-4). The authors wish to express their gratitude to Mr. Jefferson Boyles for reviewing the manuscript.

References

Alonso CD, Martins MHRB, Romano J, Godinho R (1997) São Paulo Aerosol Characterization Study. J Air Waste Manage Assoc 47: 1297–1300

Andrade F, Orsini C, Maenhaut W (1994) Relation between aerosol sources and meteorological parameters for inhalable atmospheric in São Paulo city, Brazil. Atmos Environ 28(14): 2307–2315

Brankov E, Rao T, Porter PS (1998) A trajectory-cluster-correlation methodology for examining the long-range transport of air pollutants. Atmos Environ 32(9): 1525–1534

Camargo R, Silva Dias PL (2000) The mesoscale adjustment in Paranaguábay: Case study of the period 10 to 25 August 1993. Rev Bras Meteorol (in Portuguese) 15(1): 1–13

Cape JN, Methven J, Hudson LE (2000) The use of trajectory cluster analysis to interpret trace gas measurements at Mace Head, Ireland. Atmos Environ 34: 3651–3663

Castanho ADA, Artaxo P (2001) Wintertime and summertime São Paulo aerosol source apportionment study. Atmos Environ 35: 4889–4902

Cavalcanti IFA, Marengo JA, Satyamurty P, Nobre CA, Trosnikov I, Bonatti JP, Manzi AO, Tarasova T, Pezzi LP, D′Almeida C, Sampaio G, Castro CC, Sanches MB, Camargo L (2002) Global climatological features in a simulation using the CPTEC-COLA AGCM. J Climate 15(21): 2965–2988

CETESB (2000) Relatório de qualidade do ar no Estado de São Paulo. São Paulo 1999

CETESB (2004) Relatório de qualidade do ar no Estado de São Paulo. São Paulo 2003

Clark TL, Farley RD (1984) Severe downslope windstorm calculations in two and three spatial dimensions using anelastic interactive grid nesting: A possible mechanism for gustiness. J Atmos Sci 41: 329–350

Clark TL, Hall WD (1991) Multi-domain simulations of the time dependent Navier-Stokes equations: Benchmark error analysis of some nesting procedures. J Comp Phys 92: 456–481

Cotton WR, Pielke RA, Walko RL, Liston GE, Tremback C, Jiang H, McAnelly RL, Harrington JY, Nicholls ME, Carrio GG, McFadden JP (2003) RAMS 2001: Current status and future directions. Meteorol Atmos Phys 82: 5–29

Freitas SR, Longo KM, Silva Dias MAF, Artaxo P (1996) Numerical modeling of air mass trajectories from the biomass burning areas of the Amazon basin. Ann Acad Bras Sci 68 (Suplemento 1) (in Portuguese)

Freitas SR, Silva Dias MAF, Dias PLS, Longo KM, Artaxo P, Andreae MO, Fischer HS (2000) A convective kinematic trajectory calculation for low-resolution atmospheric models. J Geophys Res 105: 375–386

Gesch DB, Verdin KL, Greenlee SK (1999) New land surface digital elevation model covers the Earth. EOS Transactions AGU 80(6): 69–70

Harrington JY (1997) The effects of radiative and microphysical processes on simulated warm and transition season

Arctic stratus. Ph.D. Diss., Atmospheric Science Paper No. 637, Department of Atmospheric Science, Colorado Sate University, Fort Collins, CO 80523, 289 pp

Herrmann P, Hanel G (1997) Wintertime optical properties of atmospheric particles and weather. Atmos Environ 31(24): 4053–4062

Innocentini V (1999) A successive substitution methods for the evaluation of trajectories approximating the parcel path by a linear function of space and time. Mon Wea Rev 127: 1639–1650

Kuo HL (1974) Further studies of the parameterizations of the influence of cumulus convective on large-scale flow. J Atmos Sci 31: 1232–1240

Landulfo E, Papayannis A, Artaxo P, Castanho ADA, Freitas AZ, Sousa RF, Viera Junior ND, Jorge MPMP, Sánchez-Ccoyllo OR, Moreira DS (2003) Synergetic measurements of aerosols over São Paulo, Brazil using LIDAR, sunphotometer and satellite data during the dry season. Atmos Chem Phys 3: 1523–1539

Liston GE, Pielke RA (2001) A climate version of the regional atmospheric modeling system. Theor Appl Climatol 68: 155–173

Louis JFA (1979) A parametric model of vertical eddy fluxes in the atmosphere. Bound Layer Meteor 17: 187–202

Lupu A, Maenhaut W (2002) Application and comparison of two statistical trajectory techniques for identification of source regions of atmospheric aerosol species. Atmos Environ 36: 5607–5618

Man CK, Shih MY (2001) Identification of sources of PM_{10} aerosols in Hong Kong by wind trajectory analysis. J Aerosol Sci 32: 1213–1223

Mellor GL, Yamada T (1982) Development of a turbulence closure model for geophysical fluid problems. Rev Geophys Space Phys 20(4): 851–875

Miranda RM, Andrade MF, Worobiec A, Grieken RV (2002) Characterisation of aerosol particles in the São Paulo metropolitan area. Atmos Environ 32: 345–352

Montero L, Vasconcellos PC, Souza SR, Pires MAF, Sánchez-Ccoyllo OR, Andrade MF, Carvalho LRF (2001) Measurements of atmospheric carboxylic acids and carbonyl compounds in São Paulo City, Brazil. Environ Sci Technol 35: 3071–3081

Pettersen S (1940) Weather analysis and forecasting. New York: McGraw-Hill, pp 221–223

Pielke RA, Cotton WR, Walko RL, Tremback CJ, Lyons WA, Grasso LD, Nicholls ME, Moran MD, Wesley DA, Lee TJ, Copeland JH (1992) A comprehensive meteorological modeling system – RAMS. Meteorol Atmos Phys 49(1–4): 69–91

Poissant L, Bottenheim WJ, Roussel P (1996) Multivariate analysis of a 1992 SONTOS (The Southern Ontario Oxidant Study) data subset, in Canada. Atmos Environ 30(12): 2133–2144

Sánchez-Ccoyllo OR, Andrade MF (2002) The influence of meteorological conditions on the behaviour of pollutants concentrations in São Paulo. Environ Pollut 116: 257–263

Saldiva PHN, Pope CA, Schwartz J, Dockery DW, Lichtenfels AJ, Salge JM, Barone I, Bohm GM (1995) Air pollution and mortality in elderly people: a time-series study in São Paulo, Brazil. Arch Environ Health 50: 159–163

Salvador P, Artíñano B, Alonso DG, Querol X, Alastuy AS (2004) Identification and characterisation of sources of PM10 in Madrid (Spain) by statistical methods. Atmos Environ 38: 435–447

Seibert PC (1993) Convergence and accuracy of numerical methods for trajectory calculations. J Appl Meteor 32: 558–566

Silva Dias MAF, Machado AJ (1997) The role of local circulations in summertime convective development and nocturnal fog in São Paulo, Brazil. Bound Layer Meteorol 82: 135–157

Smagorinsky J (1963) General circulation experiments with the primitive equations. Part I: the basic experiment. Mon Wea Rev 91: 99–164

Stauffer DR, Seaman NL (1994) Multiscale four-dimensional data assimilation. J Appl Meteor 33: 416–434

Stohl A (1996) Trajectory statistics – a new method to establish source-receptor relationships of air pollutants and its application to the transport of particulate sulfate in Europe. Atmos Environ 30(4): 579–587

Stohl A (1998) Computation, accuracy and applications of trajectories. A review and bibliography. Atmos Environ 32(6): 947–966

Tsuang B (2003) Quantification on the source/receptor relationship of primary pollutants and secondary aerosols by a Gaussian plume trajectory model: Part I: theory. Atmos Environ 37: 3981–3991

Tremback CJ (1990) Numerical simulation of a mesoscale convective complex: model development and numerical results. Ph.D. Diss., Atmospheric Science Paper No. 465, Colorado State University, Dept. of Atmospheric Science, Fort Collins, CO 80523

Vasconcellos PC, Zacarias D, Pires MAF, Pool CS, Carvalho LRF (2003) Measurements of polycyclic aromatic hydrocarbons in airborne particles from the metropolitan area of São Paulo City, Brazil. Atmos Environ 37: 3009–3018

Walko RL, Tremback CJ, Pielke RA, Cotton WR (1995) An interactive nesting algorithm for stretched grids and variable nesting ratios. J Appl Meteor 34: 994–999

Walko RL, Cotton WR, Meyers MP, Harrington JY (1995) New RAMS cloud microphysics parametrization. Part I: the single-moment scheme. Atmos Res 38: 29–62

Woodruff SD, Diaz HF, Elms JD, Worley SJ (1998) COADS release-2 data and metadata enhancements for improvements of marine surface flux fields. Phys Chem Earth 23(5–6): 517–526

Corresponding author's address: Maria de Fátima Andrade, Departamento de Ciências Atmosféricas, Instituto de Astronomia, Geofísica e Ciências Atmosféricas – IAG, Universidade de São Paulo, Rua do Matão 1226, 05508-900, São Paulo, SP, Brazil (E-mail: mftandra@model.iag.usp.br)